JOURNAL OF CATALYSIS 148, 9–21 (1994)

CO Hydrogenation on a Nickel Catalyst

I. Kinetics and Modeling of a Low Temperature Sintering Process

M. Agnelli,* M. Kolb,*,† and C. Mirodatos*

*Institut de Recherches sur la Catalyse, 2 Avenue Albert Einstein, 69626 Villeurbanne Cédex, France, and †Ecole Normale Supérieure de Lyon, 46 Allée d'Italie, 69364 Lyon Cédex 07, France

Received October 25, 1993; revised January 26, 1994

Sintering of a Ni/SiO_2 catalyst was studied under methanation conditions. The loss of metallic surface, accounting for the catalyst deactivation, was shown to come from the migration of nickel subcarbonyl adspecies formed during the reaction. The catalyst, presenting initially a monomodal Ni particle size distribution, evolved towards a bimodal system consisting of small spherical and large faceted crystals, with a selective development of ⟨111⟩ planes after several hours under reaction conditions. The formation of a nickel carbide monolayer could interfere with the formation of the large particles, possibly by decreasing the concentration of the mobile subcarbonyl adspecies.

The best description of the observed sintering process was provided by considering a model with two distinct species, evolving according to the Ostwald-ripening mechanism, and being coupled by mass transport through the mobile nickel subcarbonyl intermediates. Long-term simulations allowed for the prediction of the ultimate state of the catalyst, and solutions aimed at slowing down the loss of nickel surface were proposed.

INTRODUCTION

The commercial production of methane from syngas now has a lower priority than it did during the 1970s because numerous new natural gas fields have been discovered in the meantime. However, the methanation reaction remains an important process in the complex broad-based industrial C_1 chemistry. Moreover new environmental concerns have recently renewed interest in the direct synthesis of hydrocarbons from syngas (1). The basic reaction of CO hydrogenation, methanation, has been thoroughly studied for the past few decades, generally over nickel-based catalysts in the temperature and pressure range 200–500°C and 1000–7000 kPa, respectively (2). A major problem encountered for processes based on this reaction remains the deactivation of catalysts, which may be caused by coking, metal sintering, or poisoning phenomena (3, 4). In a previous study (5) we have shown that, in the absence of poisoning (for example as might be due to sulfide compounds or traces of heavy metal in the reacting feed), the deactivation of supported nickel catalysts actually can be considered to be due to a complex combination of particle sintering and deposition of carbon. A preliminary investigation of the sintering phenomenon, reported in (6), established that during low temperature CO methanation on Ni/SiO_2 the initially well-dispersed small Ni particles had slowly grown. The nickel transfer from particle to particle was likely due to the formation of mobile nickel carbonyl species, in agreement with the observation of Van Stiphout (3). Among the different theoretical models for sintering available in the literature, generally derived for high temperature processes, none has been found to apply directly to the particle growth kinetics found at low temperatures, possibly because of the additional complexity of this low temperature sintering mechanism (6). The present study consists of both experimental and modeling approaches to study nickel sintering aimed at understanding its origin and possibly predicting the long-term evolution of methanation catalysts. The second part of this work focuses on the changes in surface reactivity induced both by morphological changes and carbon deposition. New insights into the mechanism of CO hydrogenation may thus be gained (7).

EXPERIMENTAL

Catalyst preparation. A 15 wt% Ni/SiO_2 catalyst was prepared by impregnating silica (Aerosil Degussa 200 m^2 g^{-1}) with $[Ni(NH_3)_6]NO_3$ according to (5). The precursor was dried in flowing O_2 at 150°C for 4 h, then crushed to powder and reduced *in situ* in flowing H_2 at 650°C for 15 h, the temperature being raised at 2°C mn^{-1}.

CO hydrogenation. The methanation reaction (H_2/CO = 2) was carried out at 230°C (with additional runs at 200 and 450°C to check temperature effects) and at atmospheric pressure in a fixed bed flow reactor. From gas analyses carried out by on-line gas chromatography

0021-9517/94 $6.00

(TCD and FID) at the reactor outlet, it was observed that the selectivity in methane was around 90% (the remaining 10% being higher hydrocarbons and traces of oxygenates) and fairly stable with time on stream. We maintained a degree of conversion low enough (<10%) to ensure that differential and isothermal conditions were achieved. It being observed that the degree of conversion was proportional to the contact time (function of the weight of catalyst or the syngas flow rate) it was deduced that external diffusion was not limiting conversion; moreover, the silica support being nonporous, any significant internal diffusion could be discarded. Catalytic runs were always started with a fresh catalyst. After various times on stream, the reactor was flushed with helium and cooled to room temperature. The used samples were then analyzed by magnetic measurements, electron microscopy, volumetric H_2 chemisorption, and X-ray diffraction. For the case of magnetic measurements and volumetric H_2 chemisorption, the CO hydrogenation was carried out in a special cell which enabled simultaneous reaction and *in situ* characterization (5).

Magnetic measurements. The magnetic measurements, based on the Weiss extraction method (8), were performed in an electromagnet providing fields up to 21 kOe. The extent of nickel reduction and any possible loss of nickel during the reaction were determined from the saturation magnetization. For nickel particles remaining in the superparamagnetic domain (diameter <15 nm), two average diameters of particles were determined: D_1 at high fields corresponding to small particles, and D_2 at low fields corresponding to large particles (9).

Transmission electron microscopy (TEM). In order to get images suitable for establishing accurate particle size distributions, the catalyst was embedded in Epon resin, then cut into sections thinner than 50 nm. Highly contrasted micrographs were thus obtained on a JEOL JEM 100CX instrument. Each histogram was worked out from a statistical analysis of size measurement of about 1000 particles. Additional experiments were carried out on a VG STEM instrument.

Volumetric H_2 chemisorption. These experiments were carried out at room temperature in conventional volumetric equipment. Typically, equilibrium pressure was varied between 0 and 250 mbar.

The used catalysts were treated under flowing hydrogen at reaction temperature to eliminate eventual carbon deposits and outgassed in vacuum for 1 h at 400°C, prior to the H_2 adsorption experiments. The metallic surface area (S) was calculated from irreversible hydrogen uptake (Q_{H_2}) assuming a stoichiometry of one hydrogen atom per surface nickel atom and a site density of 14.8 atoms/nm^2 (based on an equal distribution of the three lowest index planes of nickel). The average crystallite diameter (D) was evaluated using the equation, based on a model of spherical particles (10),

$$D[\text{nm}] = 0.6/\rho S,$$

where ρ = nickel density = 8.9×10^{-4} g cm^{-3} and S = metallic surface area [m^2 g^{-1} of Ni].

X-ray diffraction. Fresh and aged samples were transferred to the XRD cell after being passivated under a flowing mixture of 1% O_2 in He at room temperature. X-ray diffraction scans were obtained using a Phillips PW1710 diffractometer with a Cu$K\alpha$ radiation and a monochromator to decrease the Kβ radiation. The metal particle size was estimated from the X-ray line broadening using the Scherrer equation (11).

Measurements were performed in a 2θ interval from 34.995 to 85.005° with a step of 0.010° and a counting time of 10 s, to ensure a precise determination of the half-height line broadening. Particle size determination by means of this technique was limited to particles larger than 5 nm.

BET measurements. The surface area of the catalysts was determined by nitrogen adsorption in an automated system, the relative pressure being fixed between 0.2 and 0.3.

EXPERIMENTAL RESULTS

Changes in silica support. In order to detect any possible change in the support morphology and texture during the CO/H_2 reaction, the contribution to surface area of the silica support was determined after various times on stream; it was evaluated from the overall BET surface area of the samples corrected by the contribution of the nickel particles (the metallic surface area was determined by volumetric H_2 adsorption) (Table 1). As can be seen, no significant variation was induced by the reaction.

Evolution of the metallic surface area. The changes of the metallic surface area and the average nickel particle size during CO/H_2 reaction were first measured by volumetric H_2 chemisorption (after carbon elimination) and the results are shown in Table 2.

TABLE 1

BET Surface Area of Ni/SiO_2 (Total Surface Area and Silica Surface Area after Correction for the Metallic Nickel Surface Area) as a Function of Time on CO/H_2 Stream at 230°C

Time on stream (h)	Total surface (m^2/g)	Silica surface (m^2/g)
0	261 ± 10	237 ± 10
4	250 ± 10	240 ± 10
16	254 ± 10	247 ± 10

TABLE 2

Amount of Irreversibly Adsorbed Hydrogen, Q_{H2}, Metallic Surface Area S, and Average Diameter D, as Determined by H_2 Volume as a Function of Time on CO/H_2 Stream at 230°C, after Coke Elimination

Time on stream (h)	Q_{H_2} irrev. (μmole/g)	S (m^2/g_{Ni})	D (nm)
0	293	164	4.1
1	215	120	5.6
3	135	75	9.0
5.5	97	54	12.4
16	94	52	12.8
96	64	37	18.1

It is noteworthy that the amount of adsorbed hydrogen for the fresh catalyst is in good agreement with the values reported in the literature for catalysts with similar characteristics (12). Moreover, the average size of the nickel particles determined by this technique, 4.1 nm, is in excellent agreement with the values obtained both from electron microscopy (3.8 nm in Table 3) and from magnetic measurements (average diameter $D_1 + D_2/2 = 4.25$ nm, Table 4). These results validate the basic assumptions of the volumetric method.

During methanation, a continuous decrease of the metallic surface area and a steady increase of the average size of the nickel particles are observed, as shown in Table 3. After checking that the nickel content remains unchanged with time (confirmed both by magnetic measurements on aged samples, after treatment with hydrogen to eliminate carbon, and by chemical analysis), it may be concluded that a nickel sintering phenomenon occurs during the reaction. This has already been pointed out in (5, 6).

Figure 1 represents a comparison of the changes in metallic surface area (curve b) and catalytic activity (curve a) as a function of time on stream. The curves, normalized with respect to their initial values ($t = 0$ h for the surface and $t = 5$ min for the activity measurements), present similar trends: a fast drop at the beginning of the reaction (during the first 3–5 h on stream) followed by a slower decay at longer times. The resemblance between the two curves suggests that the metallic surface decay largely contributes to the catalyst deactivation observed under methanation conditions.

TABLE 3

Average Size (Largest Dimension) of Small and Large Particles, Determined by Electron Microscopy as a Function of Time on CO/H_2 Stream at 230°C

Time on stream (h)	Small particles (nm)	Large particles (nm)
0	3.8	—
0.08	4.6	—
1	5.1	—
3	5.3	29.3
16	6.2	45.0
96	6.0	68.0

TABLE 4

Changes in Particle Diameters Determined by Magnetic Measurements, as a Function of Time on CO/H_2 Stream and Reaction Temperature

Time on stream (h)	T = 200°C		T = 230°C		T = 450°C	
	D_1(nm)	D_2(nm)	D_1(nm)	D_2(nm)	D_1(nm)	D_2(nm)
0	3.8	4.7	3.8	4.7	3.8	4.7
1	3.9	5.8	3.7	5.1	3.9	4.7
3	3.7	7.1	3.8	5.7	3.7	4.9
5.5	—	—	3.9	6.8	3.9	4.8

On Figure 1, curve c, the amount of carbon deposits (C atoms/surface Ni atom), measured after the reaction by temperature programmed hydrogenation, is reported as well (this point will be detailed in part II of the present study, Ref. (7)). These carbon deposits are hydrogenated into methane at the reaction temperature (around 240°C) and interact chemically with the nickel, as proved by the magnetic measurements (a nickel atom interacting with an adatom such as carbon can no longer participate in the collective ferromagnetism of a metal particle (8)). This ratio C/surface nickel atom (accounting for the particle sintering) was found to increase within about 3 h on CO/

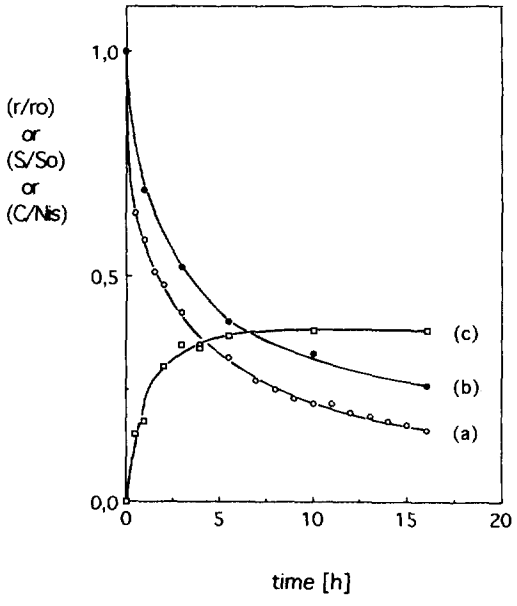

FIG. 1. Normalized changes in catalytic activity (a), metallic surface (b), and C/Ni_S (deposited carbon atom/surface nickel atom) (c) as a function of time on CO/H_2 stream at 230°C.

H_2 stream, and to stabilize at a value of around 0.38 (i.e., 2.6 Ni per C) without any noticeable further evolution. Within the experimental uncertainties and considering the physicochemical characteristics of that type of carbon (high reactivity towards hydrogen, chemical interaction with metallic nickel), it is proposed that the stabilized C/Ni_S value corresponds to the completion of a monolayer of surface nickel carbide, Ni_3C. This conclusion agrees well with the magnetic measurements showing that the equivalent of one monolayer of Ni atoms ceased to participate to the collective ferromagnetism after the catalytic run. It will be shown in part II of this study that the loss

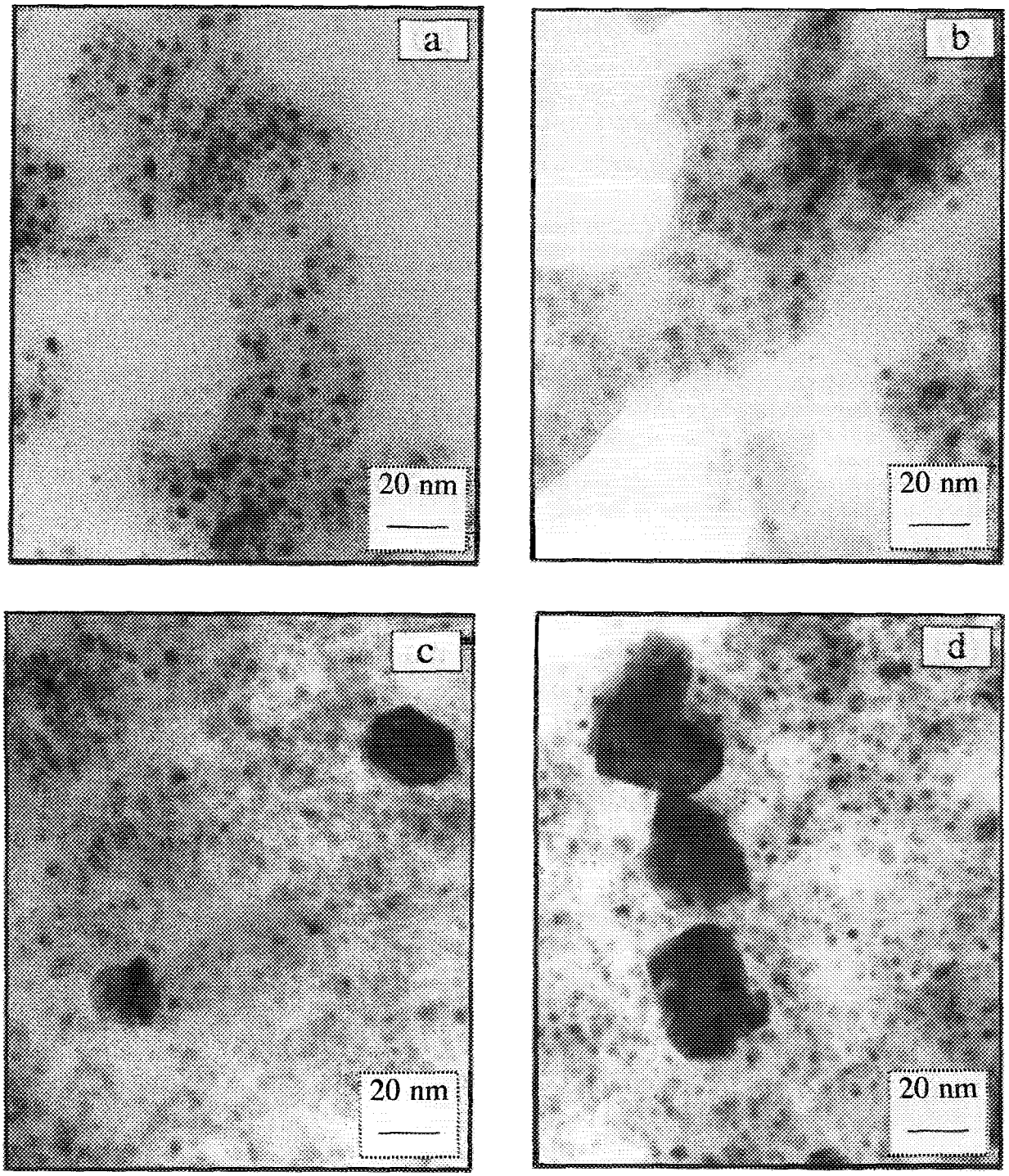

FIG. 2. TEM micrographs of Ni/SiO_2 after reduction (a), and after 1 h (b), 3 h (c), and 96 h (d) on CO/H_2 stream at 230°C.

of activity which cannot be directly assigned to the drop in the geometrical surface area (the difference between curves a and b) is related to a complex combination of that surface carbidation and the change in surface reactivity due to particle faceting (7).

Evolution of the morphology and the particle size distribution. Figures 2a–2d show the micrographs of the fresh and aged (1, 3, and 96 h on methanation stream at 230°C) catalysts. These micrographs reveal the changes in particle size and shape during the reaction. Initially, the nickel particles are small (3–4 nm), spherical, and uniformly distributed on the support. After 1 h on stream they appear to be less contrasted and slightly larger (4–5 nm). After 3 h on stream, large particles with more or less well-defined surface planes or facets (10–30 nm) appear, along with the small particles that do not change in size. The large particles steadily grow (10–100 nm), even after 96 h on stream, apparently along preferential directions (as will be confirmed by the XRD analysis), tending to form rectangle parallelepipeds. The anisotropic growth of the large particles may be interpreted as a faceting effect. At the same time the small particles remain more or less spherical in shape, although a minor faceting effect cannot be excluded. The limited resolution of the microscope prevents a more quantitative analysis.

The magnetic measurements are consistent with the conclusion from microscopy that large particles are formed and coexist with the remaining small ones. While D_1, the diameter related to the small superparamagnetic particles, remains rather stable with time on stream, D_2, the diameter chartacteristic of the larger particles, slowly increases as shown in Table 4 (T = 230°C). It may be noted that after about 3 h of reaction, a remanent magnetization (remaining magnetization when the applied field was suppressed) develops, evidence that some nickel particles have reached a diameter larger than the "critical value" (around 15 nm) above which they cannot be considered to be superparamagnetic any longer (8, 9). Under these conditions, D_2 no longer relates to the true particle diameter.

Particle size distributions (PSD), normalized separately for the small and the large particles, are obtained from micrographs for different times on stream and are presented in Fig. 3. Table 3 shows the mean diameters of both the small and the large particles, as calculated from the micrographs. As previously stated, the PSD for t = 0 h is narrow with an average particle size of 3.8 nm, in agreement with volumetric H_2 chemisorption results (Table 2). Immediately after the reaction mixture is admitted onto the catalyst (t = 5 min), the PSD slightly shifts to larger sizes (average size of 4.6 nm). After 1 h on stream, the particles continue to grow (average size of 5.1 nm). After 3 h on stream a second distribution of large particles develops (average size of 29.3 nm), while the initial distributions slowly broadens. For still larger times on stream (t = 16 and 96 h) the PSD of the large crystallites steadily shifts to larger values and spreads out (average size of 45.0 and 57.2 nm, respectively), while the PSD of the small particles remains practically unchanged (average size around 6.0 nm).

Let us emphasize that the combined PSD of small and large particles presents the form of a bimodal distribution with two well-defined maxima. This observation suggests that two distinct types of particles with separate distributions (obtained from micrographs with different magnifications) coexist for reaction times larger than 3 h.

Influence of the temperature on the particle size evolution. Table 4 shows the evolution of the particle size as determined by magnetic measurements for reaction temperatures 200, 230, and 450°C. The data clearly show that the lower the reaction temperature, the faster the sintering process, as already pointed out in (6).

Particle counting. The total number of particles may be obtained directly from the micrographs. However, because of the large dispersion of particle sizes, it was obviously impossible to obtain good statistics for all particle sizes from the same type of micrograph (compare for instance Figs. 2c and 2d, where there is only one, respectively, three large particles for more than a thousand small ones).

Therefore, *in a first step*, small and large particles have been counted separately on micrographs, with magnification adapted to the corresponding particle size. The "windows" used for the counting have been chosen at random in order not to bias the determination of either type of particles. The number of particles per window turned out to be almost constant, allowing for a reliable extrapolation to the whole surface and a quantitative evaluation of the number of each type of particles per unit surface area. This separate counting reveals the two following features:

—The number of small particles diminishes with time on stream (while their size hardly varies beyond 3 h on stream as seen in Table 3).

—The number of large particles remains almost constant as soon as they appear after approximately 3 h on stream (while their size increases steadily between 3 and 96 h).

In a second step, both types of particles were counted together (in view of modeling the sintering phenomenon):

—When only small particles are present (from 0 to 3 h on stream), their number per unit BET surface area can be determined simply from the metallic and the BET surfaces, from the size distribution, and by assuming that the particles are spherical (as observed by electron microscopy).

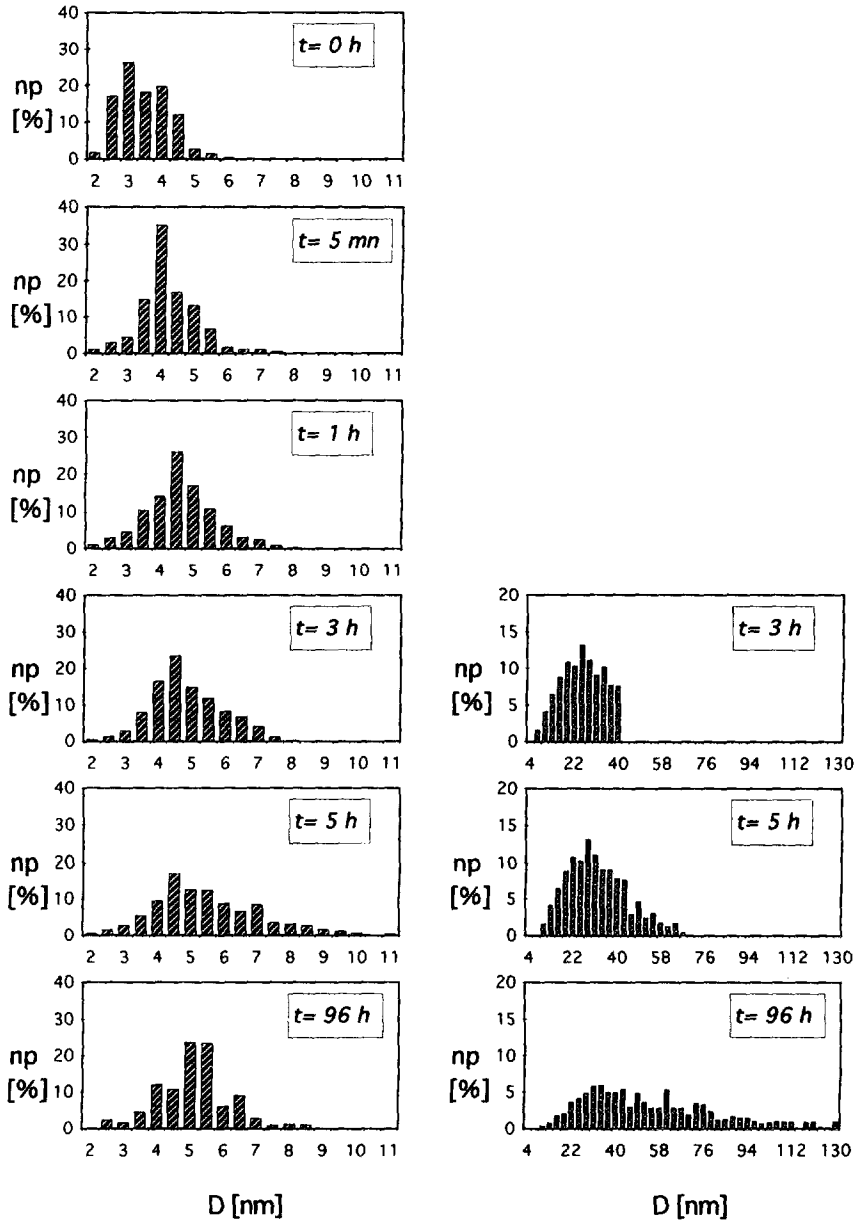

FIG. 3. Normalized particle size distributions determined from TEM micrographs as a function of time on CO/H_2 stream at 230°C.

—At t = 3 h, the large particles have already appeared and their number remains approximately constant thereafter. As the large particles are far less numerous than the small particles (between two and three orders of magnitude as estimated from the micrographs), it may be assumed that, for short times on stream, the metallic surface area of the large particles can be neglected compared with that corresponding to the small particles. Therefore, the number of small particles can be evaluated as for the previous case. From this number, the amount of nickel (%) corresponding to the small particles can be deduced.

Concerning the large particles, their number can then be estimated from (i) the corresponding amount of nickel (obtained by difference between the total amount and the amount corresponding to the small particles), (ii) the normalized size distribution obtained from the TEM images (Fig. 3, right column), and (iii) a geometrical model.

Because of the occurrence of faceting and because the large particles have preferential growth directions, a spherical model is not appropriate. Instead, a rectangular parallelepiped has been chosen as a simple, acceptable model crystal habit for these particles, consistent with the micrographs. The average aspect ratio length/width (a/b) of these particles was directly evaluated from the micrographs and the corresponding values for different times are reported in Table 5. Assuming an arbitrary value

TABLE 5

Dimensions of the Rectangle Parallelepiped Model of the Large Particles (a = Length, b = Width, c = Height, Dimensionless Values Normalized to the Mean Length of the Large Particles at t = 3 h) as a Function of Time on CO/H_2 Stream at 230°C

Time on stream (h)	a/b	a	b	c
3	1.1	1	0.9	0.9
16	1.2	1.5	1.3	0.6
96	1.4	2.3	1.6	0.4

of a = 1 for t = 3 h, it was straightforward to deduce the value of b, and the third dimension of the rectangle parallelepiped c (inaccessible to direct observation by TEM) was then calculated in order to satisfy the previously verified conditions: (i) the number of large particles, once present, remains constant and (ii) the total quantity of nickel is conserved during the experiment. The values of the three dimensions a, b, and c of the geometrical model thus determined are reported in Table 5.

The number of small and large particles determined on the basis of the above model is reported in Table 6. Analysis confirms that the ratio of the large particle number to the small particle number remains small over the range of experimental observation, even though the number of small particles is continuously decreasing, as anticipated from the direct TEM observation.

From the separate size distributions for large and small particles (Fig. 3) and from the overall particle counting (Table 6), a single, combined particle size distribution may be produced. It is presented on a logarithm scale in Fig. 4. This distribution, initially monomodal, evolves clearly towards bimodal after 3 h on stream, with two well-defined maxima, as suggested previously from the qualitative TEM analysis. This important feature will have to be taken into account by any modeling.

TABLE 6

Number of Particles per BET Surface Area Unit and Percentage of Nickel Corresponding to the Small and Large Particles of Time on CO/H_2 Stream at 230°C

Time on stream (h)	Small particles		Large particles	
	Diameter (nm)	Ni%	Diameter (nm)	Ni%
0	2446	100	0	0
1	1012	100	0	0
3	574	64	1.5	36
16	322	52	1.5	48
96	245	32	1.5	68

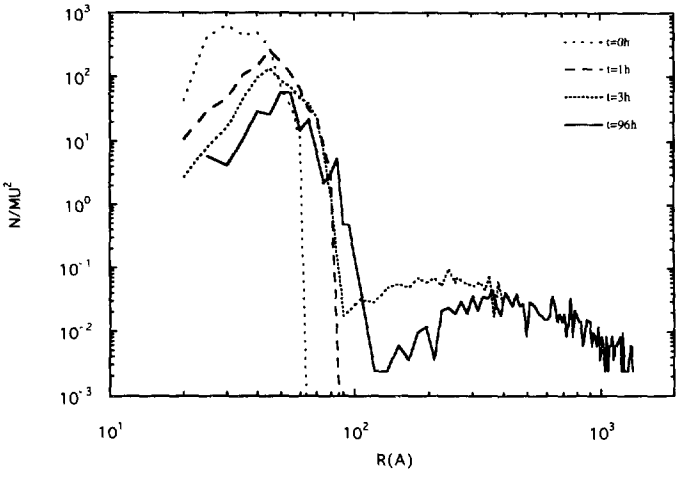

FIG. 4. Evolution of the global particle size distribution determined from T.E.M. micrographs and particle counting as a function of time on CO/H_2 stream at 230°C.

Crystallographic evolution of the particles. In order to illustrate the morphological changes of the larges particles, a schematic representation of the large particles in the framework of the simple model presented above has been drawn in Fig. 5 based on the normalized a, b, and c values reported in Table 5. It appears very clearly that the particles tend to flatten and grow along a preferential direction during the sintering process, in accordance with the direct analysis of TEM images.

In order to quantify this crystallographic evolution, X-ray diffraction experiments have been carried out on differently aged samples. The data corresponding to fresh and aged samples are presented in Fig. 6. The spectrum

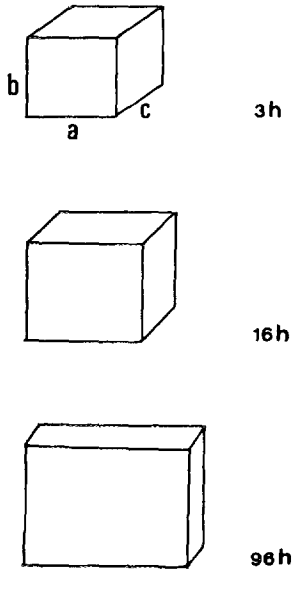

FIG. 5. Schematic representation of the large, faceted particles after 3, 16, and 96 h on stream, modeled as a rectangular parallelepiped.

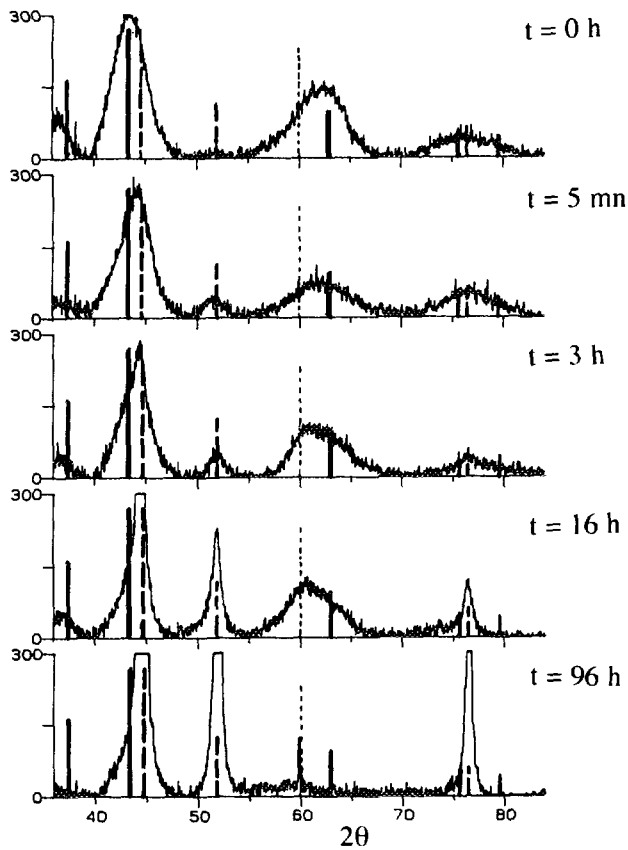

FIG. 6. Ni/SiO_2 XRD patterns as a function of time on CO/H_2 stream at 230°C. Patterns of pure Ni^0 (dashed line) and NiO (solid line) are superimposed.

of the fresh catalyst corresponds to a NiO pattern indicating that the metallic nickel particles have been reoxidized during the exposure of the sample to air, despite the passivation procedure. The spectra of the aged catalysts are the superposition of the Ni^0 and the NiO patterns, which evince a stronger resistance to reoxidation. Although a detailed quantitative analysis is not possible, it may be seen that the ratio of Ni^0 to NiO increases with reaction time and that, after 96 h on stream, the aged sample is almost exclusively composed of Ni^0.

The main diffraction peaks of the sample aged for 96 h correspond to ⟨111⟩, ⟨200⟩, and ⟨220⟩ planes of metallic nickel. Their profiles which present a very broad base and a sharp peak at the reflecting angle are typical of a bimodal particle size distribution: the broad part is due to the small particles and the narrow part is due to the large particles (11). The relative amount of nickel corresponding to small and large particles and the average particle size, as estimated from the surface and the width at half-height of the deconvoluted peaks, are presented in Table 7 for the samples aged for 16 and 96 h (X-ray diffraction patterns of the less aged catalysts are not exploitable due to massive nickel oxide formation). At t = 96 h about 33% of the total nickel is present as small particles having a mean diameter of 5 nm, while the rest is in the form of large crystals of 10–100 nm. These results are in good agreement with TEM data (Table 3) and magnetic measurements.

TABLE 7

Average Diameter of Ni Particles and Percentage of Nickel Corresponding to the Small and Large Particles as Determined by XRD as a Function of Time on CO/H_2 Stream at 230°C

Time on stream (h)	Small particles		Large particles	
	Diameter (nm)	Ni%	Diameter (nm)	Ni%
16	5	50	10–100	50
96	5	33	10–100	67

TABLE 8

XRD Pattern Characteristics of the Sample Aged for 96 h

Diffraction angle (rad)	Peak intensity (a.u.)	L ⟨*hkl*⟩	Half-height width (rad)
44.55	100	⟨111⟩	0.3
51.89	42	⟨200⟩	0.6
76.44	21	⟨220⟩	0.6

Examination of the half-height width (Table 8) of the sharp peaks shows that the large particles are anisotropic, as the half-height width for the ⟨111⟩ plane is half of that corresponding to the other orientations. Thus, particle faceting of nickel during CO/H_2 reaction tends to favor the development of dense ⟨111⟩ planes. This fact supports the geometric model proposed for the large particles and its evolution as a function of the time of reaction (Fig. 5). These ⟨111⟩ planes are very likely the predominantly exposed faces for catalysis.

DISCUSSION

Nature of the sintering process. During the methanation reaction at low temperature on a Ni/SiO_2 catalyst, deactivation appears to be related mostly to the decrease of the metallic surface due to particle sintering. However, other processes such as carbon deposition may also contribute to the loss of catalytic activity (7).

The sintering process only concerns the metallic phase of the catalyst as the support remains stable during the reaction. The evolution of the particle size distribution, from monomodal to bimodal after several hours on stream, does not, by itself, allow one to determine which mechanism is responsible for the sintering process: particle migration and coalescence or atomic migration be-

tween immobile particles. The observation that small particles coexist with large faceted ones even after a long time on stream and the progressive disappearance of the small particles is consistent with either mechanism. For the case of the atomic migration model, particles smaller than the initial ones (i.e., <1 nm) should be observed after coarsening; unfortunately, the direct observation of particles smaller than 1 nm is not possible with the available TEM equipment for the Ni/SiO_2 system.

A clear indication in favor of the atomic migration model is provided by complementary experiments carried out on $NiCu/SiO_2$ catalysts. When a homogeneously alloyed $NiCu/SiO_2$ catalyst (presenting a metal loading close to that of Ni/SiO_2, 14 wt%) was exposed to the same reaction conditions, a similar type of sintering was observed: large faceted particles were formed at the expense of small ones. STEM analysis of the samples, reported in Table 9, shows unambiguously that:

(i) on the initial sample the copper content, either averaged over a large number of particles (column 2) or determined for a single particle (column 3), is very close to the overall chemical content (around 13 at%), which demonstrates the good homogeneity of the alloy,

(ii) after 16 h on stream, the average copper content stays unchanged, but the large faceted particles are composed almost exclusively of nickel (2% Cu), while the small particles are enriched with copper by comparison with their initial composition (17%).

Only an atomic and selective extraction of nickel from the small particles and its subsequent deposition on the large particles can explain this observation.

It is shown in Table 4 that the lower the reaction temperature, the faster the nickel sintering. This feature rules out any physical process, such as particle migration and coalescence, which would be favored by temperature, and moreover expected to occur at temperatures close to or higher than the Tammann temperature (590°C for nickel). Therefore, a chemical process has to be considered for this low temperature sintering phenomenon. It was already shown in Ref. (5) that the sintering is CO pressure dependent but is insensitive to the presence of other gases such as H_2O or CH_4, and it was concluded that nickel was likely to be transported by means of carbonyl or subcarbonyl species. The observed relationship between sintering rate and temperature reinforces this hypothesis. It is well established that the equilibrium of the reaction $Ni^0 + 4\ CO \rightleftharpoons Ni(CO)_4$ is shifted towards the decomposition of nickel carbonyl when temperature increases (K_p is 9.5×10^{-6} and 7.5×10^{-12} at 500 and 800 K, respectively) (13, 14). The chemical extraction of nickel by means of carbonyl-type species also explains why only nickel is transported during sintering of a NiCu alloy, since the actual P_{CO} and T conditions are not favorable to the formation of copper carbonyl.

TABLE 9

Chemical Composition on a Ni–Cu/SiO_2 Catalyst Determined by STEM Nanoanalysis, Either Averaged on a Large Number of Particles or Related to Individual Small and Large Particles, as a Function of Time on CO/H_2 Stream at 230°C

Time on stream (h)	Average Cu(wt%)	Individual particle Cu(wt%)	
		Small	Large
0	13.8	12.6	—
16	13.2	16.5	2.1

The following additional information may help to better explain the nature of the migrating species and the sintering process:

(i) no net loss of nickel from the catalytic bed has ever been observed under the present reaction conditions. Therefore it seems unlikely that the nickel is transported as gaseous $Ni(CO)_4$ from particle to particle.

(ii) Liang *et al.* (15) have observed by means of pulsed field desorption mass spectrometry that the species formed during nickel single crystal fragmentation under CO (10^{-6} to 2×10^{-2} Pa at 270–370 K) were primarily mono-, bi-, and tri-carbonyl adspecies and not the gaseous $Ni(CO)_4$, the highest concentration being observed for the $Ni(CO)_2$ species.

(iii) by means of isotopic transient kinetics, the amount of CO reversibly adsorbed on the catalyst under the present reaction conditions has been determined: a ratio CO/surface Ni atom of 2.1 was found as soon as the Ni/SiO_2 sample was brought in contact with the reaction mixture (part II of this work, Ref. (7)). The observation is consistent with the formation of the dicarbonyl adspecies detected by Liang *et al.* (15).

In view of these results, it is proposed that in the present case of nickel sintering the migrating species are the intermediate subcarbonyl adspecies (mostly dicarbonyl ones) and that they migrate on the silica surface thus ensuring nickel interparticular transport. This process will also guarantee nickel mass conservation, as was observed in our experiments.

In summary, the nickel phase during methanation at low temperature after several hours on stream can be described in terms of a condensed phase forming a bimodal distribution of small (roughly spherical) and large (faceted) particles coexisting with an atomically dispersed phase of subcarbonyl adspecies which ensures the interparticular nickel transfer.

Surface restructuring. Sintering not only induces particle growth but also a crystallographic restructuring of

the nickel particles: dense ⟨111⟩ planes develop at the expenses of less dense planes such as ⟨200⟩ and ⟨220⟩.

Schmidt *et al.* (16) studied the dissolution of a hemispherical Ni single crystal reacting with CO by field ion microscopy. Faceting of the nickel crystals with a selective increase of the ⟨111⟩ planes was observed at low CO pressure (2 mbars) and at 100°C. It was inferred that atomic extraction of Ni from the lattice is easier from incomplete chains of ⟨111⟩ planes, leading to the disappearance of surface defects and therefore to the development and smoothing of these planes. The higher reactivity of atomic defects on the ⟨111⟩ planes is attributed to the fact that these atoms can accommodate up to three CO bondings while only two bonds are possible on less dense planes. More generally, Greiner and Menzel (19) have shown that the initial roughness of the surface was favorable to the nickel carbonylation.

These observations suggest that the ability of a surface nickel atom to be carbonylated and extracted from the crystal is a function of the surface defects of the crystal. Assuming a higher reactivity between CO and Ni atoms in defect positions on ⟨111⟩ planes, it may be inferred that for the present case of nickel sintering under methanation conditions, the formation/migration/decomposition of mobile subcarbonyl adspecies results in the formation and smoothing of the ⟨111⟩ planes as experimentally observed for the large particles.

Effect of surface carbidization on nickel sintering. An important feature of the sintering process is that the large particles, which may be interpreted as a distinct species with their own growth rules and size distribution, start to appear only after about 3 h on stream with CO/H_2. On the other hand nickel transfer from particle to particle occurs as soon as the catalyst is brought into contact with the CO/H_2 reaction mixture (leading to an immediate change in the small particle distribution). This apparent lag between the immediate nickel transfer process between small particles and the appearance of the large faceted particles suggests that there exists a distinct phenomenon, characterized by relatively slow kinetics, which initially interferes with the sintering process that results in the formation of the largest particles.

This phenomenon could be the nickel surface carbidization since one notices a striking coincidence of the completion of the surface carbide layer Ni_3C after 3 h on stream (curve c in Fig. 1) and of the appearance of the large particles.

The influence of nickel carbidization on CO adsorption has been thoroughly investigated on single crystals. McCarty and Madix (17) and Bertolini and Tardy (18) have clearly demonstrated that on ⟨111⟩ and ⟨110⟩ nickel surfaces, the presence of superficial carbide markedly lowers the bond strength of CO; it may even entirely suppress adsorption on the ⟨100⟩ surface. Moreover, on the carbided Ni(110)C surface, only linear CO is observed (18). In addition, Greiner and Menzel (19) have observed that the carbidization of a clean Ni ⟨100⟩ surface was highly detrimental to $Ni(CO)_4$ formation.

These facts support the idea that there is a relationship between the carbidization and the appearance of the faceted particles. Let us assume that the carbidization tends to slow down the formation of surface subcarbonyl species. According to the previously quoted literature, this phenomenon should affect the regularly ordered nickel atoms of the smooth planes more strongly than the nickel atoms in defect positions. Accordingly, if one considers that the small spherical particles present a higher density of defect atoms than the faceted particles (whatever their size), it may be deduced that the carbidization will inhibit the carbonyl formation to a larger extent on the faceted particles than on the small rough ones. This could explain that the process of surface carbidization is likely to accelerate the transfer of nickel from the small spherical particles to the largest faceted ones. It also might explain the observed coupling between surface carbidization and the development of large faceted particles.

Modeling. There are two models that have been proposed in the literature for particle sintering in catalysis: (i) the kinetic model of particle migration and coalescence (20) and (ii) the thermodynamic Ostwald-ripening model of atomic species migration (21, 22). Both models describe systems with a monomodal particle size distribution upon sintering. However, the present case is fundamentally different, as the initially monomodal distribution clearly evolves towards a bimodal distribution.

Let us summarize the mechanisms that we have investigated in view of explaining the spontaneous appearance of a bimodal size distribution. The models include Monte Carlo simulations of a modified atomic diffusion model, kinetic coarsening of a single species with size-dependent growth kinetics and kinetic coarsening of two separate species with different kinetic coefficients. The details of the numerical investigation will be presented elsewhere (23).

Monte Carlo simulation. Modeling was first attempted by means of Monte Carlo simulations of a lattice gas. In contrast with standard atomic models, the diffusion coefficient for the atoms of the vapor phase (atomically dispersed nickel subcarbonyl species) differs from that of atoms diffusing on particle surfaces. Furthermore, atomic evaporation from irregular surfaces is facilitated in comparison with evaporation from flat surfaces. These assumptions tend to favour smoothing of the large particles surfaces and enhance the net rate of condensation on such facetted crystals (23). The appearance of facets in the simulations can be compared with the faceting observed

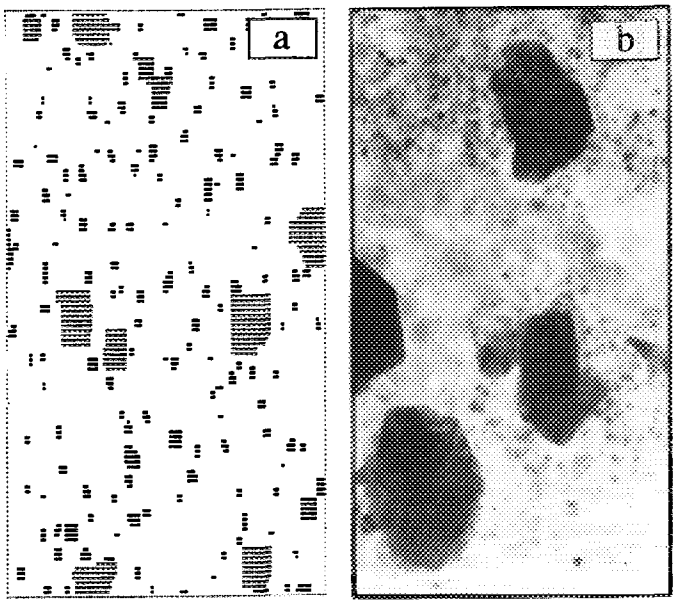

FIG. 7. Comparison between a Monte Carlo simulation (a) and an experimental TEM image after 96 h on CO/H_2 stream at 230°C (b).

in the experiments, notably the pronounced faceting of the ⟨111⟩ planes. The result of such a simulation is shown in Fig. 7a and compared with a TEM image of a sintering experiment (Fig. 7b). The qualitative agreement between computation and experiment is quite good; nevertheless there is an important difference between experiment and simulation: the experiments develop a true bimodal size distribution at late stages, whereas the simulations merely produce a broad monomodal distribution.

Thermodynamic model. Modeling was also attempted on the basis of Ostwald ripening but including modifications to favor the appearance of large particles. The modifications consisted of either (i) an abrupt change of the supersaturation (concentration of the atomically dispersed nickel subcarbonyl species around the particles) to model the transition from the thermal (nickel sintering under hydrogen, negligible at 230°C) to the chemical (nickel sintering under CO/H_2) coarsening process in the experiments or (ii) an explicit modification of the size dependence of the coarsening rate. In case (i) the supersaturation re-equilibrates before any significant particle growth takes place, thus excluding any qualitative change of the size distribution, and in case (ii) only a broadening of the distribution is achieved, similar to the Monte Carlo simulation discussed above. Even a permanent freezing of the supersaturation of the atomic species (which corresponds to fixing the surface concentration of the subcarbonyl species on the silica support) would not produce a bimodal size distribution: the small particles disappear more rapidly than the large ones appear.

To model bimodal size distributions, we are therefore led to consider models with two different species. This can be motivated by the different surface properties of the two types of Ni particles.

Two-species model. A generalized kinetic (or thermodynamic) model with two separate species with different growth dynamics and coupled by means of the vapor phase has been studied by numerically solving the kinetic equations. The difference between the two species is introduced through different coefficients for the evaporation/condensation rates. Starting initially with a distribution of small particles, the large particles nucleate and then grow at the expense of the small particles. A bimodal size distribution analogous to that found in the experiments is observed at intermediate times.

Unfortunately, we do not have any detailed experimental information as to how the faceted particles nucleate. Because of this uncertainty we modeled the appearance of the second phase by atomic nucleation. While the mechanism of nucleation is all-important for the early stages of the coarsening, it probably does not influence the late stages, when the two species are in thermodynamic equilibrium. Let us discuss two possible cases:

(i) initially, the system is constituted of small spherical nickel particles and a phase of metallic monomers of nickel subcarbonyls, on a flat substrate (silica surface). The faceted large particles nucleate from the monomers. The data clearly show the coexistence of the two species as a transitory phenomenon: the large particles grow at the expense of the small ones, which eventually disappear (Fig. 8),

(ii) the surface properties of some (randomly chosen) spherical particles change and transform them into faceted

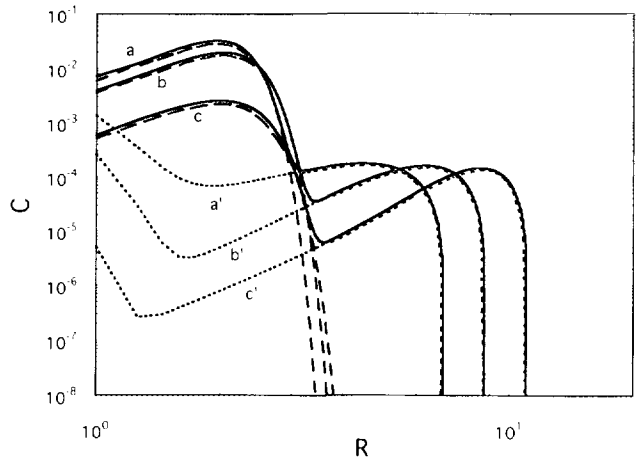

FIG. 8. Evolution of the particle size distribution (particle concentration vs particle radius) as a function of three successive times on stream (a,a'; b,b'; c,c' in arbitrary units), calculated on the basis of a two-species kinetic model with different evaporation/condensation coefficients for the two types of particle. a, b, c (dashed line): spherical particles; a', b', c' (dotted line): faceted particles. Solid line: total size distribution.

particles. At early stages, this leads to the coexistence of spherical and faceted particles of comparable size (indistinguishable by TEM because of the limited resolution of the microscope). This is consistent with the observations by Schmidt *et al.* (16), who exposed Ni single crystals to CO.

In Fig. 9, the appearance of a bimodal distribution in the context of random nucleation is sketched (23): due to different surface energies for the small and the large particles, the critical radius R_C, which separates shrinking from growing particles in the framework of the Ostwald-ripening model, is different for the two types of particles, $R_{C,S}$ (for small particles) $> R_{C,L}$ (for large particles). All the faceted particles grow, whereas, after the initial nucleation period, all the small particles shrink because the common supersaturation (and the critical radii) equilibrates at a value intermediate between those corresponding to the two types of particles. A gradual change of the supersaturation from the small to the large particle value is expected. This evolution tends to enhances the preferential growth of the facetted particles with time and leads to a more pronounced bimodal size distribution (Fig. 9, top to bottom).

Sintering based on the explicit two-species model is consistent with the following experimental observations:

(i) a bimodal distribution appears after a finite time. This delay may be related to the changes in solid/vapor phase equilibria, induced by the slow process of surface carbidization. As a matter of fact, this process has been shown to eventually inhibit the carbonyl formation, and therefore to decrease the vapor phase (subcarbonyl monomers) concentration. Moreover, this inhibiting effect on the carbonyl formation is likely to affect the faceted particles more severely than the small rough ones. Within the scope of the present model, these effects should slow down both the nucleation step and the large particle growth, in accordance with the experimental observations;

(ii) the number of small particles diminishes while their size does not change significantly, until most of the mass has been transferred to the large particles;

(iii) the size of facetted particles, once nucleated, increases but their number remains essentially constant.

As much longer times can be reached in the simulations than in the experiments, the model can be used to predict that the bimodal size distribution represents a transitory state which eventually leads to the complete disappearance of the small particles and to a standard Ostwald-ripening growing process of the facetted particles.

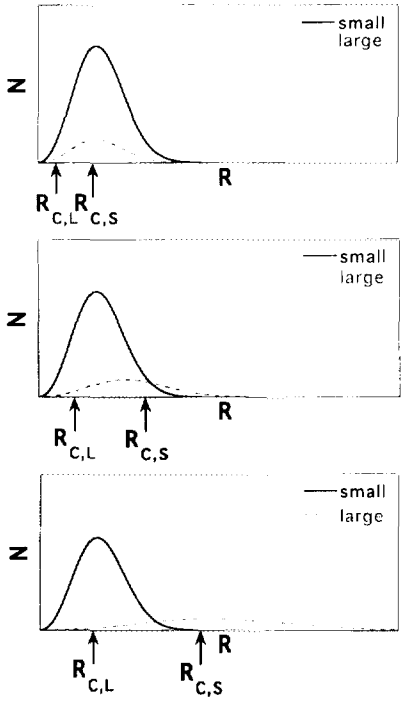

FIG. 9. Sketch of the appearance and evolution in time (from top to bottom) of a bimodal distribution for Ostwald ripening, for two species with different surface energies.

CONCLUSIONS

Sintering of a Ni/SiO_2 catalyst was studied under methanation conditions. Our study has revealed that the loss of metallic surface, accounting for a major part of the catalyst deactivation, may have been due to a chemical process. Nickel transfer probably occurred by means of migration of nickel subcarbonyl adspecies formed during the reaction. The system, initially constituted of small spherical particles and presenting a monomodal size distribution, evolved towards a bimodal system consisting of small spherical and large faceted crystals, after several hours under reaction conditions. The observed formation of a complete nickel carbide monolayer after a characteristic time on stream could preferentially interfere with the formation of the large particles, possibly by markedly decreasing the concentration of the atomically dispersed and mobile subcarbonyl adspecies. This would displace the sintering equilibrium between the particles and the dispersed phase.

A selective development of ⟨111⟩ planes is another consequence of this low temperature sintering process. It will be shown elsewhere (7) that this surface restructuring markedly changes the reactivity of the nickel surface during CO hydrogenation.

Among the models investigated, the best description of the observed sintering process is provided by considering two distinct species, each evolving according to the thermodynamic Ostwald-ripening mechanism, but with different surface properties, and being coupled by mass transport through a mobile nickel subcarbonyl intermediate.

This model successfully described the main features observed experimentally.

A remaining open question is how exactly the faceted particles nucleate. Both the carbidation of the small particles and the smoothing of the facets of the large particles may be at the origin of the nucleation of the second species.

Long-term simulations using our model predict that the small particles totally disappear and that the large ones continue to grow. From the point of view of catalysis, this trend should lead to an almost complete and irreversible deactivation of the catalyst. Based on the presently improved knowledge of the sintering process, solutions aiming at slowing down the loss of nickel surface can therefore be proposed:

(i) changes in operating conditions to render the carbonyl formation less favorable, e.g., by increasing the reaction temperature and decreasing the CO pressure;

(ii) changes in catalyst composition in order either to inhibit the *carbonyl formation* (e.g., by alloying nickel with copper as will be reported elsewhere (7)) or to inhibit the *carbonyl migration* between metal particles (e.g., via alkali addition which tends to stabilize the carbonyl species on the support and therefore prevent particle growth, as observed on the related cobalt systems (24)).

REFERENCES

1. Saint-Just, J., Basset, J. M., Bousquet, J., and Martin, G. A., *Recherche* **21,** 222 (1990).
2. Vannice, M. A., *Cat. Rev.—Sci. Eng.* **14,** 153 (1976).
3. Van Stiphout, P. C. M., PhD thesis, The Netherlands, 1987.
4. Bartholomew, C. H., *Catal. Rev.—Sci. Eng.* **24**(1), 67 (1982).
5. Mirodatos, C., Praliaud, H., and Primet, M., *J. Catal.* **107,** 275 (1987).
6. Agnelli, M., Kolb, M., Nicot, C., and Mirodatos, C., *in* "Catalyst Deactivation 1991" (C. H. Bartholomew and J. B. Butt, Eds.), p. 605. Elsevier, Amsterdam, 1991.
7. Agnelli, M., and Mirodatos, C., in preparation.
8. Selwood, P. W., "Chemisorption and Magnetization." Academic Press, New York, 1975.
9. Primet, M., Dalmon, J. A., and Martin, G. A., *J. Catal.* **46,** 25 (1977).
10. Gregg, S. J., and Sing, K. S. W., *in* "Adsorption, Surface Area and Porosity." Academic Press, London 1982.
11. Klug, H. P., and Alexander, L. E., *in* "X-Ray Diffraction Procedures," Wiley–Interscience, London, 1954.
12. Bartholomew, C. H., and Pannell, R. B., *J. Catal.* **65,** 390 (1980).
13. Shen, W. H., Dumesic, J. A., and Hill, C. G., *J. Catal.* **68,** 152 (1981).
14. Rostrup-Nielsen, J. R., and Hojlund Nielsen, P. E., *in* "Deactivation and Poisoning of Catalysts" (J. Oudar and H. Wise, Eds.), p. 259. Dekker, New York, 1985.
15. Liang, D. B., Abend, G., Block, J. H., and Kruse, N., *Surf. Sci.* **126,** 392 (1983).
16. Schmidt, W. A., Block, J. H., and Becker, K. A., *Surf. Sci.* **122,** 409 (1982).
17. McCarty, J. G., and Madix, R. J., *Surf. Sci.* **54,** 121 (1976).
18. Bertolini, J. C., and Tardy, B., *Surf. Sci.* **102,** 131 (1981).
19. Greiner, G., and Menzel, D., *J. Catal.* **77,** 382 (1982).
20. Pulvemacher, B., and Ruckenstein, E., *AIChE J.* **19,** 1286 (1973), and *J. Catal.* **29,** 224 (1973).
21. Wynblatt P., and Gjostein, N. A., *Prog. Solid State Chem.* **9,** 1 (1975).
22. Flynn, P. C., and Wanke, S. E., *J. Catal.* **37,** 432 (1975).
23. Kolb, M., Agnelli, M., and Mirodatos, C., to be published (Note: Readers interested in details of the modelling prior to publication may contact one of us (M. Kolb)).
24. Dalmon, J. A., Chaumette, P., and Mirodatos, C., *Catal. Today* **15,** 101 (1992).